High-performance discharges in the Small Tight Aspect Ratio Tokamak (START)

D. A. Gates, R. Akers, L. Appel, P. G. Carolan, N. Conway et al.

Citation: Phys. Plasmas **5**, 1775 (1998); doi: 10.1063/1.872819
View online: http://dx.doi.org/10.1063/1.872819
View Table of Contents: http://pop.aip.org/resource/1/PHPAEN/v5/i5
Published by the American Institute of Physics.

High-performance discharges in the Small Tight Aspect Ratio Tokamak (START)*

D. A. Gates,[†,a)] R. Akers, L. Appel, P. G. Carolan, N. Conway, J. Dowling, M. Gryaznevich, T. Hender, O. J. Kwon,[b)] R. Martin, M. Nightingale, M. Price, C. Roach, A. Sykes, M. R. Tournianski, M. Walsh,[c)] C. D. Warrick, and the START and NBI teams
UKAEA-Fusion, Culham Science, Abingdon, Oxon, OX14 3DB, United Kingdom

(Received 18 November 1997; accepted 19 January 1998)

The Small Tight Aspect Ratio Tokamak (START) [A. Sykes *et al.*, Nucl. Fusion **32**, 769 (1994)] spherical tokamak has recently achieved the record value of toroidal $\beta \sim 30\%$ in a tokamak-like configuration. The improvements that have made these results possible are presented along with a description of the global equilibrium parameters of the discharges. The ideal magnetohydrodynamic (MHD) stability of these discharges is analyzed, and they are found to be in close proximity to both the ballooning limit and the external current driven kink limit, but they are found to be far from the pressure driven external kink limit. Disruptivity for a range of shots is not correlated with the normalized β limit, but does correlate well with the empirical high-l_i disruption limit. The transport properties of these high-β equilibria are analyzed and compared to conventional tokamak scaling laws and transport models. The global transport is at least as good as that predicted by the ITER97-ELMy (edge-localized) scaling law. The local ion transport is in good agreement with that predicted by neoclassical models. The electron transport is anomalous, showing rough agreement with the Lackner–Gottardi transport model. © *1998 American Institute of Physics.* [S1070-664X(98)93305-5]

I. INTRODUCTION

Spherical tokamaks have been predicted to have several favorable properties when compared to tokamaks with a conventional aspect ratio.[1] They are compact in size, support a high natural elongation, and are predicted to have improved plasma stability. In particular, they can operate with high $\beta = 2\mu_0\langle p\rangle/B^2$, which is an important parameter in determining the efficiency of a tokamak power plant. The high limit to β is largely due to the high values of normalized current, $I_N = I_p/aB$ which can be readily achieved on spherical tokamaks. This increased stability has also been calculated using more sophisticated numerical models.[2]

The Small Tight Aspect Ratio Tokamak (START) was designed to test the spherical tokamak concept. It has been operational at Culham Laboratory since 1990, first studying the ability to maintain plasma equilibrium with high plasma temperature. High plasma current was achieved by a novel induction compression start-up scheme. Having achieved this aim, the machine has been continually improved to broaden the accessible operating regime.

Recently, experiments have been carried out on the START tokamak injecting a hydrogen neutral beam into a deuterium plasma using an injector on loan from Oak Ridge National Laboratory. These experiments have demonstrated the capability of running at high β, achieving a world record β of 32%, originally reported in Ref. 3. This exceeds the previous record $\beta = 12.6\%$, achieved on the DIII-D tokamak,[4] by well over a factor of 2. New experiments, which will be described in Secs. II and III have shown that high values of β can be maintained for several energy confinement times without a decreasing toroidal field.

The machine improvements that led up to the achievement of this record value of β will be discussed in Sec. II. Analysis of the equilibrium, stability, transport properties, and edge phenomenology will be presented in Secs. III, IV, V, and VI, respectively, along with the relevant supporting data.

II. MACHINE IMPROVEMENTS

A series of improvements to the START device has been responsible for the increase in achievable β. In particular: (1) the neutral beam power was increased, (2) the poloidal and toroidal field capacitor bank systems have been upgraded, and (3) the vacuum conditions have been improved.

The neutral beam power has been increased steadily since the initial operation of the beam.[5] The initial power injected in 1996 was ~ 300 kW. Power was optimized further to 550 kW for the first record β discharges in March of 1997. Further improvements, including the installation of a titanium getter pump in the neutralizer, have allowed for an additional increase in the available power to over 1 MW.

The capacitor banks that supply the vertical field were upgraded to provide sufficient current to maintain plasma position control in the high-β regime. Additionally, the toroidal field system was upgraded to provide ~ 10 ms of ''flat-

*Paper oThaI1-1 Bull. Am. Phys. Soc. **42**, 2002 (1997).
[†]Invited speaker.
[a)]Present address: Princeton Plasma Physics Lab, Princeton, NJ.
[b)]Taegu University, Taegu, South Korea.
[c)]Walsh Scientific, Ltd., Culham Science Centre, Abingdon, UK.

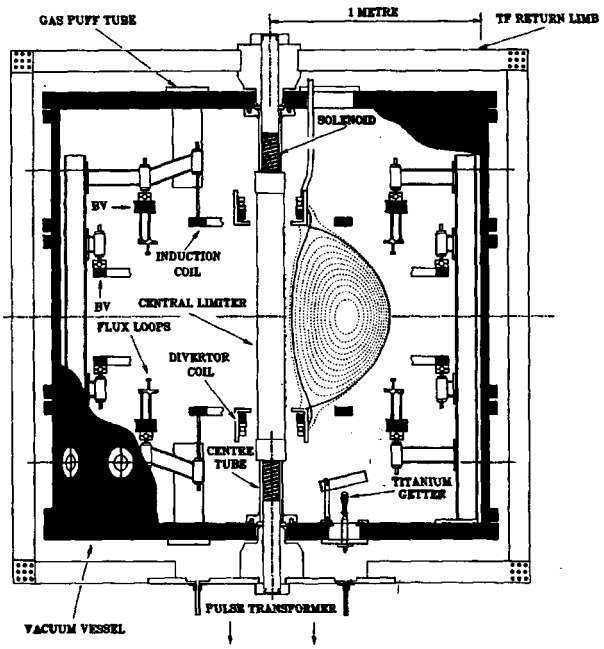

FIG. 1. Cross-section drawing of the START tokamak showing the coil locations and the location of the newly installed shrouded titanium getter. Inset is an equilibrium reconstruction of the record β plasma, shot 32993.

top'' toroidal field. This was achieved by sequentially firing two additional capacitor banks into the toroidal field circuit.

Several improvements were made to the vacuum system. An insulating jacket was added to the vacuum vessel to allow higher temperature baking. A titanium getter was installed with a line of sight shroud to prevent the coating of plasma facing components. First wall conditioning is provided by weekly boronization with trimethyl boron in a helium glow discharge and inter-shot helium glow discharge cleaning, both of which are now routinely used. These improvements have facilitated an increase in the accessible operating space for the following parameters: I_p, I_p/I_{rod}, (where I_{rod} is the current which provides the toroidal field), β, and β_N.

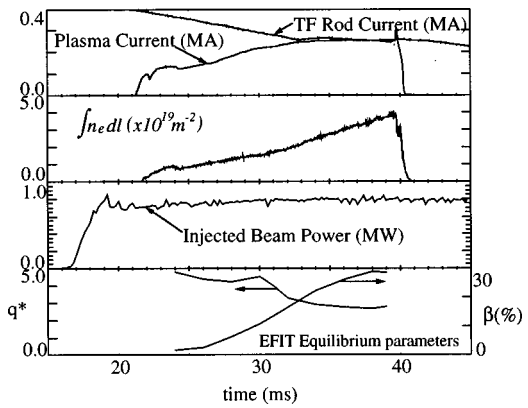

FIG. 2. Time history of the global parameters for a typical high-β discharge, shot 34237. This discharge has $I_p/I_{\mathrm{rod}} \sim 1$ for 10 ms. The plasma $\beta > 20\%$ for 6 ms$\sim 3\tau_E$.

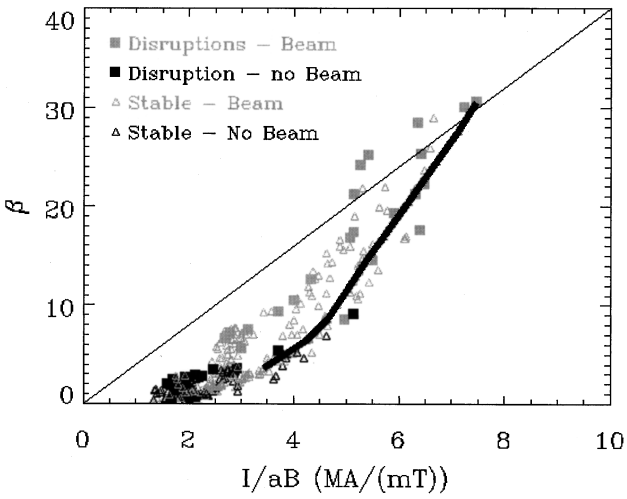

FIG. 3. Troyon diagram for a series of START equilibria, including the record β equilibria. The disruptions are not well correlated with a line in this plane. Solid squares indicate that the plasma disrupted within 1 ms of the time of equilibrium reconstruction. Open triangles indicate the equilibrium remained stable for greater than 1 ms. Black indicates an ohmic discharge, while gray indicates a beam heated discharge. Data is presented from 48 different discharges.

III. FORMATION AND EQUILIBRIUM

The plasma is formed using the induction-compression method. The plasma forms initially around the ''induction'' coils shown in Fig. 1. The plasma is then compressed to low aspect ratio by applying a vertical field using the shaping/vertical field coils. Once the plasma is formed, the solenoid is used to ramp up the current to ~ 250 kA. A high plasma current is required for good beam absorption (see Sec. V). Typically, the neutral beam is on from the very beginning of the shot, in order to maximize the heating. The plasmas formed are double null divertor discharges, with the nulls being formed around the two ''X-point'' coils. The plasma

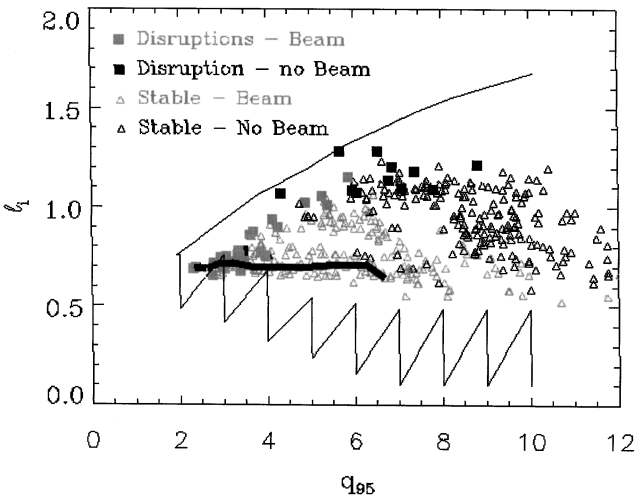

FIG. 4. The same equilibria as those in Fig. 3 in the l_i-q_{95} plane. The data are well correlated with the high-l_i region of the empirical stability boundary. This indicates that the high-β disruptions on START are likely due to the proximity to this current profile determined stability boundary, and not to the pressure driven kink boundary.

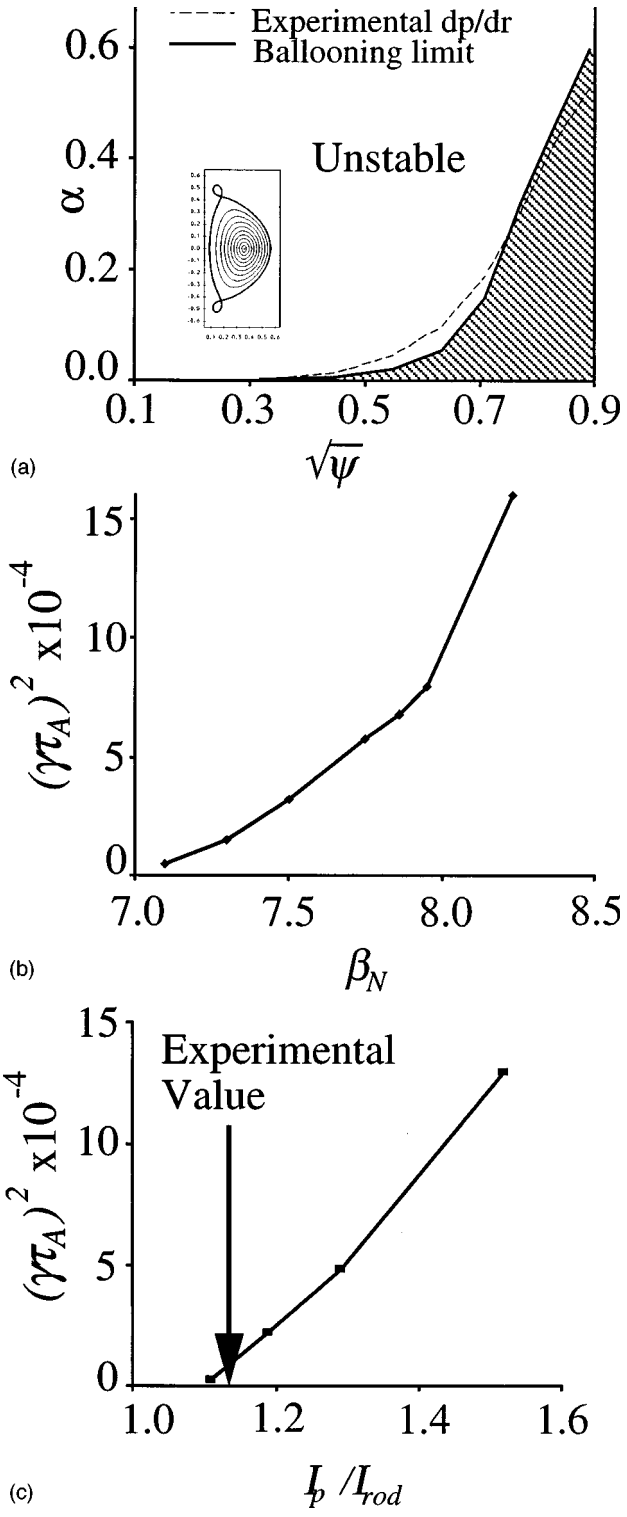

FIG. 5. Output from the ERATO ideal stability code showing (a) that the entire profile is near marginal stability for ballooning modes for shot 32993, the record β discharge, (b) the plasma is stable to pressure driven external kinks for values well above those observed in experiment, and (c) that this equilibrium is calculated to be unstable to low-n external kink modes.

density ramps up throughout the shot, due to beam fuelling and recycling, although the density ramp rate can be increased with additional gas puffing.

Figure 2 shows the time history of the global parameters for a typical high-β discharge, shot 34237. The plasma is

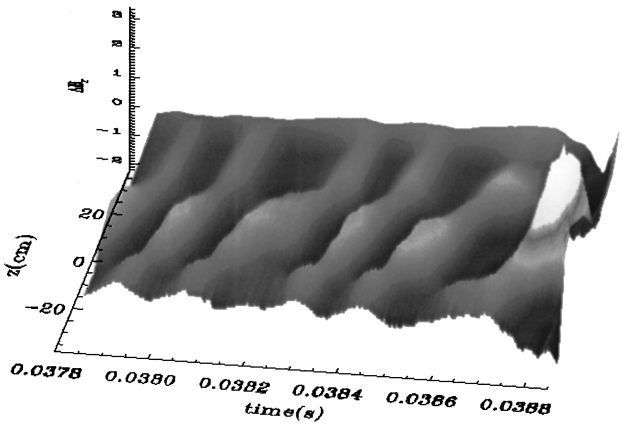

FIG. 6. Data from two vertical arrays of vertically oriented magnetic pickup coils located on the START center column, separated toroidally by 180°, which shows the growth of a large $n=1$ precursor mode to the disruption of shot 34375. The data was processed by integrating the measured dB/dt and subtracting the signals from opposing coils to give the $n=$odd component on the perturbed magnetic field.

initiated using the induction compression method at time $t=20$ ms. The neutral beam is on throughout the shot, injecting hydrogen into a deuterium plasma. The plasma current is ramped up and the toroidal field is ramped down, lowering q and raising β. The additional toroidal field banks are then fired leading to $I_p/I_{\rm rod}\sim 1$ for 10 ms. The kinetic energy ramps up steadily, then saturates before the plasma disrupts. The nature of this limit will be discussed in the section on plasma stability. The maximum plasma current to date in START is $\sim$290 kA. The maximum $I_p/I_{\rm rod}$ is 1.2 similar to that reported earlier in Ref. 3.

A typical equilibrium for the high-β discharges is shown in Fig. 1. The plasma is a double null with elongation $\kappa\sim 2$, requiring no fast vertical position control system. The aspect ratio is $A\sim 1.3$ with a plasma β of $\sim$30%. The reconstruction is from the EFIT[6] code using data from external magnetics only. The derived global parameters for all the discharges discussed are taken from similar equilibrium reconstructions. The current profile is parametrized by a fixed functional form, as is the pressure profile. The EFIT output pressure profile has been compared to kinetic measurements of the total pressure, and the difference is in good agreement with the predicted fast ion pressure.

An important issue for START is the proper specification of the eddy currents in the thick conducting wall. The wall is thick enough that not only is the L/R time important, but also the skin time. This means that the current decay time is not constant, but varies as a function of time. The model used in the present reconstructions uses data from a vacuum shot to match the measured vertical field on the central column by adjusting the overall magnitude of the ideal wall currents (that is the currents that would exist in the wall if it were perfectly conducting) with a single parameter. This correction is then similarly applied to the currents induced in the wall by the plasma. Work is ongoing to develop an independent resistive wall model to estimate the error in this method.

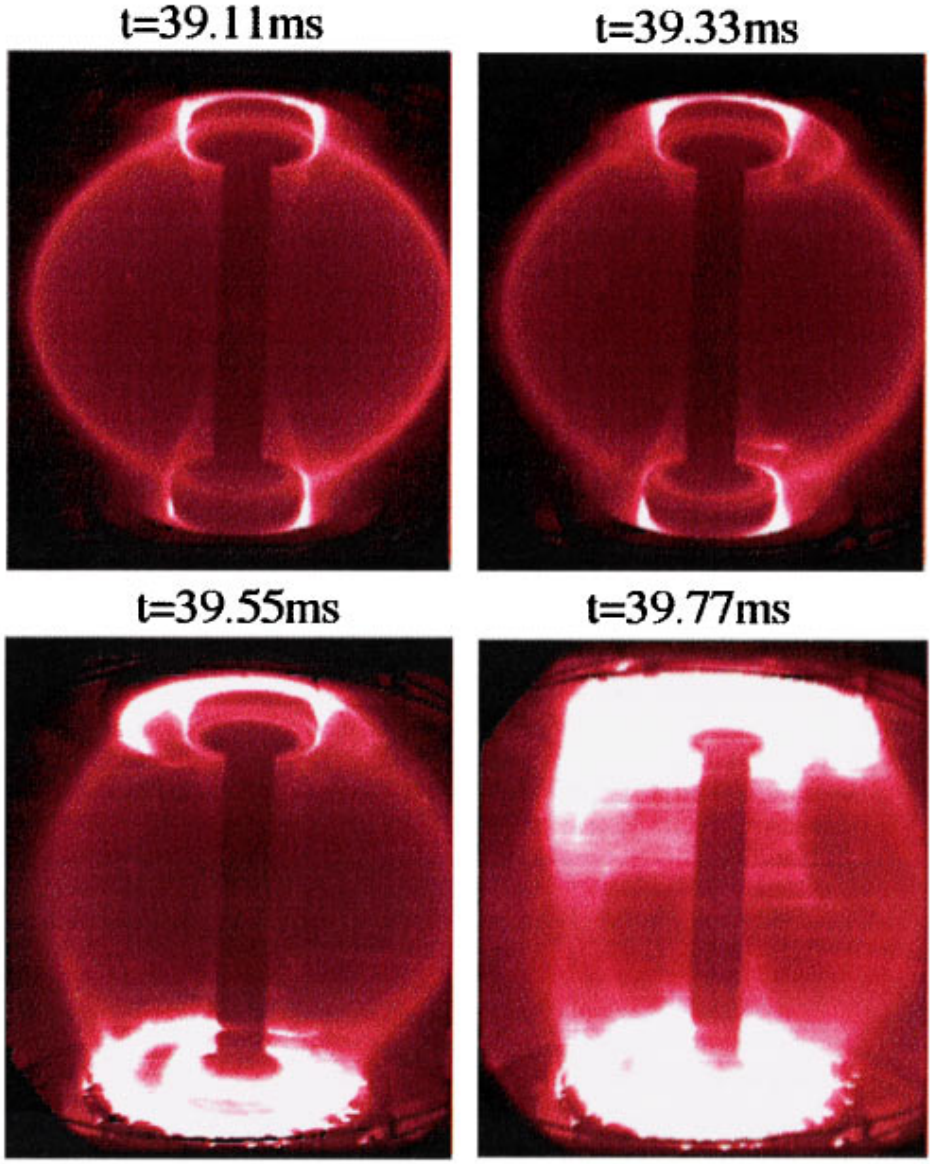

FIG. 7. High-speed video camera frames showing a large $n=1$ perturbation of the plasma boundary. The camera is located 1 m from the plasma vertical axis, and was configured to take one frame every 11 μs (4500 Hz).

IV. STABILITY

The high-β discharges presented all end in disruptions. The loss of disruption immunity was reported earlier in Ref. 5, wherein it was conjectured that the cause of this charge was the positioning of the X-point coils in close proximity to the plasma boundary. During an internal reconnection event (IRE), the change in plasma internal inductance causes a low aspect ratio plasma to increase it's elongation, rather than to cause an inward radial displacement (to first order).[7] In previous START configurations, there was no solid material to interact with above or below the plasma. With the addition of coils near the plasma boundary this freedom to expand vertically is removed. However, now that plasma pressure is high, and the safety factor low, the question naturally arises as to the cause of disruptions in the present discharges.

A simple test of whether or not a disruption is caused by a plasma being in proximity to the β limit is to lower the β and see if the plasma still disrupts. Figure 3 shows a Troyon diagram for a series of START discharges with varying parameters. Shots with neutral beam heating are shown in gray, while ohmic shots are in black. Each point represents a different equilibrium reconstruction, with data being taken from 48 different shots. It is clear from the diagram that there is not a definitive operational limit to the achievable β which is proportional to I/aB. In fact, in the Troyon plot shown, the disruptions (i.e., the last equilibrium reconstruction before a disruption), which are represented by the solid symbols, are randomly distributed amongst stable equilibria, indicating that pressure is not the key factor in determining the stability of these discharges.

An important clue as to the cause of disruptions in START is the fact that all disruptions are preceded by internal reconnection events (IREs), and that all IREs in this set of discharges occur after the time of maximum loop voltage

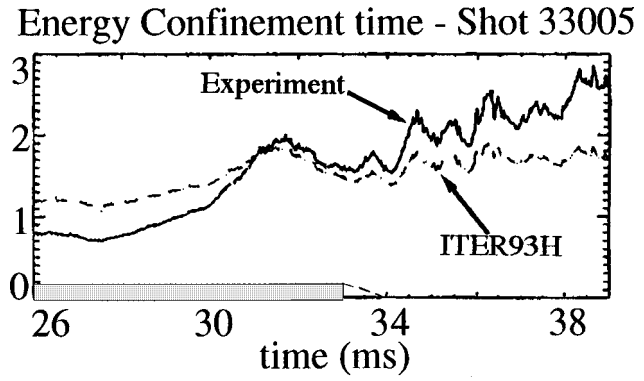

FIG. 8. Global energy confinement as calculated for shot 33005. The gas puff was shut off early in this discharge, which led to an increase in the calculated energy time, as well as interesting edge phenomena (see Sec. VI).

(in a pulsed capacitor bank driven machine, the loop voltage is often far from steady state). One of the expected effects of a decreasing loop voltage is a peaking of the current profile. Plotting l_i, the internal inductance of the plasma, a measure of the peakedness of the current profile, against q_{95} in Fig. 4 shows that there is a good correlation of the disruptions with a high l_i boundary. The boundary in the diagram is an empirical stability boundary for current driven disruptions taken from Ref. 8. The data in Fig. 4 is taken from the same equilibrium reconstructions used in the Troyon diagram of Fig. 3.

Also, theoretical calculations of the stability of the highest β discharges indicate stability to global pressure driven external kink modes. However, ballooning mode calculations indicate that the profiles are near marginal stability for much of the plasma cross section. This may indicate that the highest β discharges are at a pressure limit, but this has not been verified experimentally. The lowest q discharges are near

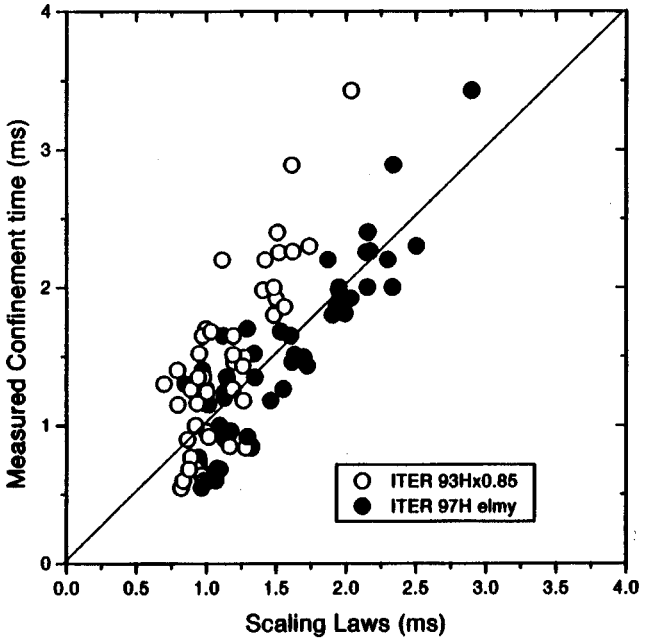

FIG. 9. Scatter plot of the measured global energy confinement time versus that predicted by the ITER93H and ITER97-Elmy scaling laws; the correlation with ITER97-Elmy is good.

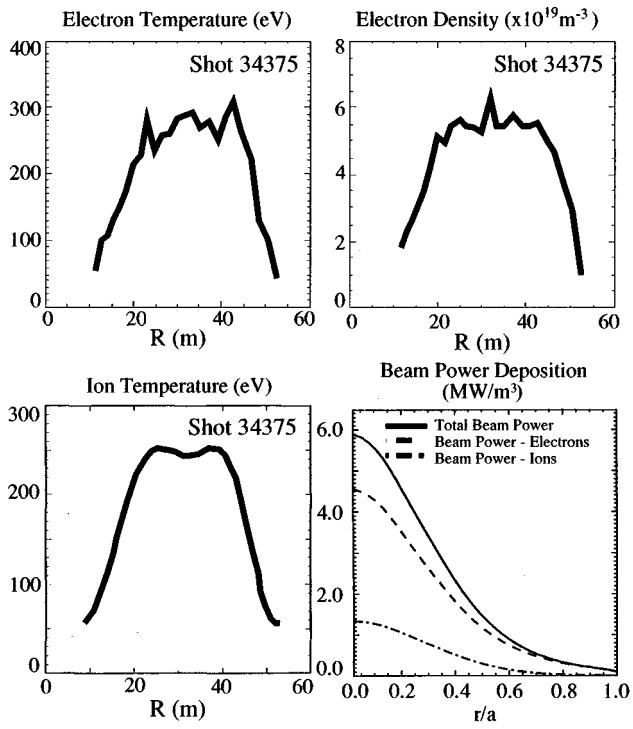

FIG. 10. Measured profiles of T_i, T_e, and n_e from shot 34375. Electron density and temperature profiles are measured using a single pulse multipoint Thomson scattering system. Ion temperatures are measured using a multichord charge exchange spectrometer. Also shown is the beam deposition profile, calculated using the measured density and temperature profiles.

marginal stability to current driven external kinks. The high-q, high-l_i disruptions are associated with internal modes. Figure 5 shows output from the ERATO[9] code supporting (a) that the entire profile is near marginal stability to ballooning modes, (b) that the plasma is stable to external pressure driven kinks for values of β well above those observed in experiment, and (c) that the equilibrium is unstable to current driven external kink modes.

Therefore, the highest β cases, which are also the lowest q cases, are near the stability margin for low-n current driven kinks. These plasmas are also at the ballooning limit, as determined using the current and pressure profiles from the equilibrium reconstructions. The l_i-q diagram indicates these discharges are also near the boundary for high-l_i internal mode driven disruptions.

To help identify which mechanism is actually responsible for the disruptions at high β, analysis of the magnetohydrodynamic (MHD) precursors of the disruptions has been performed. The measured instability eigenmode for shot 34375 is shown in Fig. 6. The colors represent the magnitude of the odd component of the vertical magnetic field perturbation, which is measured on the central rod in START with two vertical arrays of pickup coils separated toroidally by 180°. The signals from these two arrays are subtracted from each other to yield the odd toroidal mode number component. There is a clear growing $n=1$ mode present (identified by frequency) which leads up to the disruption. The presence of a low-n mode would tend to rule out the ballooning mode

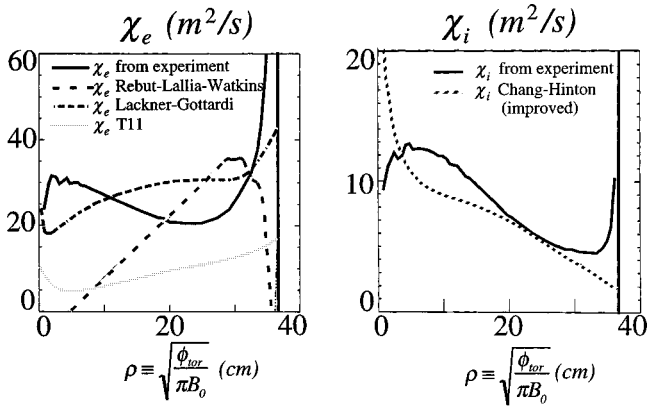

FIG. 11. Thermal diffusivity profiles as calculated using the ASTRA transport code. The calculations use the measured pressure profiles and the calculated beam deposition profiles as inputs. Z_{eff} is assumed to be 2. Also shown are the predictions of various transport models.

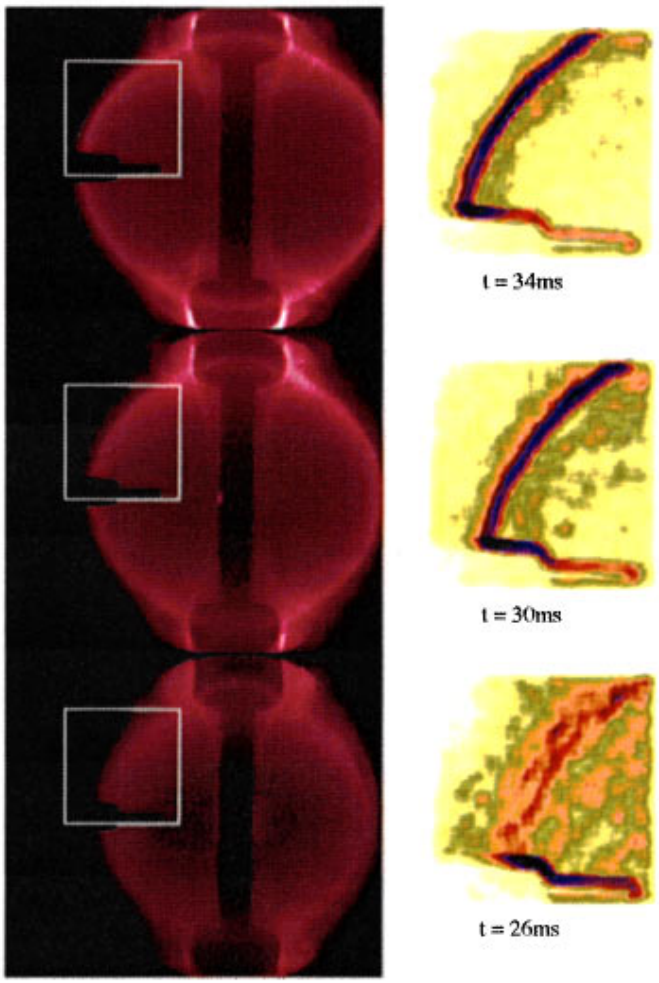

FIG. 12. Width of the visible light emission as a function of time from the high-speed video camera. The frames on the left show edge enhanced frames from the insets in the frames on the right.

β-limit scenario (at least for the low-q disruptions), but it is difficult to be certain whether this mode is a cause or an effect of the disruption due to the rapid growth rate of the mode ($\tau < 100\ \mu$s). There is additional evidence of a large low-n perturbation of the plasma boundary from the high-speed video camera. An example is shown in Fig. 7 for shot 34237.

V. ENERGY TRANSPORT

An important question for spherical tokamaks is how the transport compares to other toroidal confinement systems. START is the first low aspect ratio experiment to reach (relatively) high plasma temperature and density. Plasma temperatures in START routinely reach 400 eV, well above all relevant radiation barriers.

The global energy confinement time for a representative high-performance discharge is shown as a function of time in Fig. 8. The energy confinement time predicted by the ITER93H scaling law[10] is also shown in the figure. There is reasonable agreement between the measured and predicted values. This, in fact, is somewhat surprising, since the ITER93H scaling law is an empirical fit to confinement data that does not span the relevant aspect ratio range. However, the close agreement between the two curves indicate that the level of performance achieved in START is similar to that achieved by other tokamaks at conventional aspect ratio in high confinement mode (H-mode). Better agreement yet is achieved with the ITER97-ELMy (edge-localized mode) scaling law, as shown by the scatter plot in Fig. 9.

More sophisticated calculations of the radial dependence of energy transport have also been carried out using the measured ion temperature, electron temperature, and electron density profiles, which are routinely available on START. The ion temperatures are measured using a multichannel charge exchange spectrometer,[11] while the electron density and temperature profile are measured using a multichannel Thomson scattering diagnostic. Profiles of these quantities are shown in Fig. 10 for shot number 34375.

Also shown in the figure is the beam power deposition profile as calculated using the LOCUST[3] code. An important variable in the beam power deposition calculations is the edge neutral density. The value used has been estimated from the measured neutral particle energy spectrum from a neutral particle analyzer. The power deposition calculation uses the reconstructed equilibrium from EFIT, together with the electron density and temperature profiles from the Thomson scattering.

The beam power deposition, electron density and temperature profiles, and the ion temperature profiles are then used as inputs to the ASTRA[12] transport code. The code is used to calculate the experimental ion and electron thermal diffusivities in real geometry. The only assumed quantity is Z_{eff}, which is set uniformly to 2 across the profile. The calculated χ's are shown in Fig. 11. Also shown in the figures are the diffusivities predicted by various transport models. An improved interpretation of the[13] Chang–Hinton approximation to the neoclassical transport shows reasonable agreement with the experimental value. As in all transport calculations, the shape of the radial profile of the energy diffusivity depends on the gradients of the profiles of the stored energy. The electron energy diffusivity is substantially higher than the ion diffusivity. The Lackner–Gottardi[14]

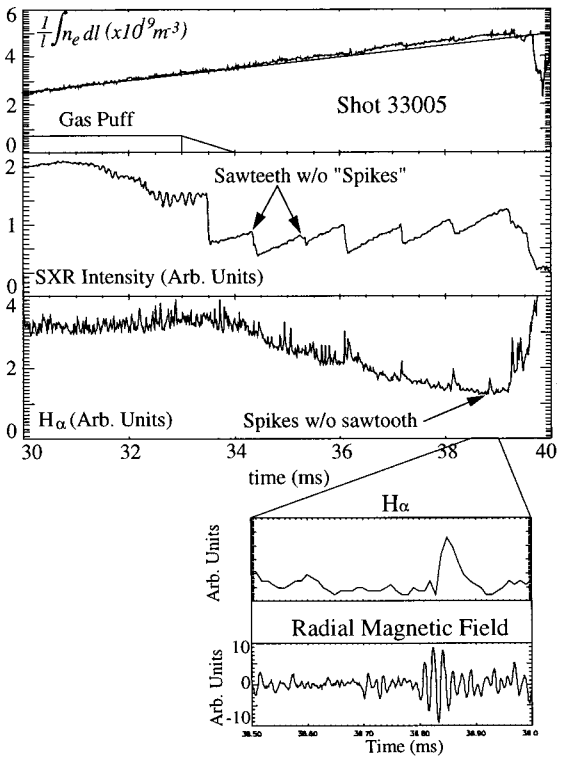

FIG. 13. Data from the central soft x-ray diode, along with edge $H\alpha$ measurements and magnetic fluctuation measurements from a moveable pickup coil just outside the plasma outboard midplane. Most of the $H\alpha$ spikes are correlated with sawteeth. However one is not, indicating it is a separate event. There is always a high-frequency magnetic fluctuation associated with the $H\alpha$ spikes, but not with sawteeth alone.

model is in rough agreement with the magnitude of the predicted electron diffusivities, but the radial dependence is not well matched. The other transport models show poor agreement with the electrons.

VI. EDGE PHENOMENOLOGY

The phenomenology of the edge of START high-performance discharges wherein the gas puff is turned off show many interesting features. In particular the following features are observed:

(1) Flat density profile with sharp edge gradients.
(2) Well-defined scrape-off layer.
(3) Density rise (without gas puff) with simultaneous $H\alpha$ drop.
(4) $H\alpha$ spikes with associated high-frequency magnetic precursors.
(5) Reduction in high-frequency magnetic fluctuation level.

(1) The density profile is extremely flat as evidenced by the Thomson scattering profile (not shown). Additionally, there is clear evidence of a very sharp edge density gradient. Exactly how sharp the gradient is is difficult to say since the density gradient scale length is on the order of or less than the Thomson scattering channel spacing, but this places an upper bound of ~ 2 cm on the gradient scale length.

(2) There is clear evidence that the scrape-off layer in these plasmas becomes narrower than in a typical START discharge. A series of frames from a high-speed video camera is shown in Fig. 12. The width of the region with high intensity visible emission is reduced by a substantial fraction $(\sim 1/2)$.

(3) There is both a drop in the $H\alpha$ level and an increase in the rate of density increase at the time of increase in energy confinement (see Fig. 8) as seen in Fig. 13. This indicates an increase in particle confinement time. Following the end of the gas puff at 33 ms, the time scale for the drop in $H\alpha$ levels is slow, $\sim 3-5$ ms. This may be due to the large excess volume of the START vacuum chamber.

(4) $H\alpha$ spikes with high-frequency magnetic precursors are clearly visible in shot 33005. Figure 13 shows the $H\alpha$ signal as measured on the midplane along with the perturbed radial magnetic field in the frequency range 50–250 kHz, as measured by a removable magnetic probe on the START outboard midplane. There is clearly a growing magnetic precursor to the $H\alpha$ spike, as is typical for edge localized modes (ELMs) seen in the H-mode in conventional tokamaks. Also, this precursor is seen preceding all the $H\alpha$ spikes in this discharge. Whereas most of the spikes are correlated with sawteeth, in most cases they spikes actually precede the sawtooth crash. Similarly, sawteeth in the discharge which do not have $H\alpha$ spikes also have no high-frequency perturbation. The spike shown in detail is not correlated with a sawtooth at all, giving the clearest indication that it is a separate phenomenon.

(5) Figure 14 shows a moving window Fourier transform of the measured radial magnetic field on the outboard midplane. There is a clear reduction in the high-frequency magnetic fluctuations in the ~ 500 kHz range at the time of the transition to the modified confinement mode. An interesting feature of the transition is the extended time scale, similar to the time scale for the reduction in $H\alpha$ light. Also, since the time scale is long, it is possible to observe a reduction in the average frequency of the fluctuations, indirect evidence for a change in plasma edge rotation at this time. The longer time scale for transition also raises the interesting possibility of making a clear determination of the chain of events that leads to improved confinement. In this shot, a small increase in the energy confinement time is observed at the time of the reduction in high-frequency magnetic activity.

These plasmas appear to be in a different confinement regime than previously reported START discharges that have peaked profiles (e.g., see Ref. 5). The exact nature of this difference requires further investigation. The fact that this regime is not readily observed with the gas puff on is an important clue as to the nature of the changed confinement regime.

VII. SUMMARY

Improvements to the START experiment have widened the accessible operating space, culminating in the achievement of the world record plasma β in a tokamak, $\beta = 32\%$. These improvements include: (a) an increase in the auxiliary heating power, (b) enhancements to the poloidal field power supplies, and (c) improvements to the vacuum vessel conditioning system. In addition to the record β, the following

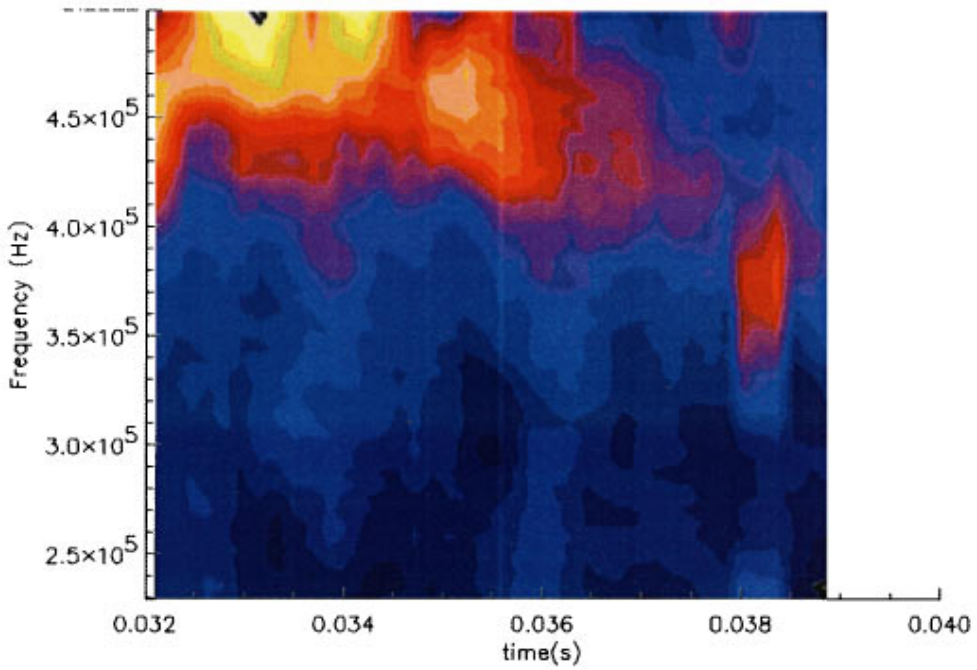

FIG. 14. Moving window Fourier analysis of the high-frequency magnetic fluctuation spectrum of shot 33005, where bright colors represent high amplitude. There is a clear reduction in the size of the high-frequency fluctuation amplitude at the time of the increase in energy confinement. There is also a noticeable reduction in the frequency of the fluctuations, indirect evidence for a change in plasma edge rotation. The bright broad spectrum at time 38 ms is due to a sawtooth correlated with an $H\alpha$ spike.

parameters have also been achieved: (1) $I_p/I_{\mathrm{rod}}=1.2$, (2) $I_p=290$ kA, (3) $q_{95}=2.3$, and (4) $\beta_N=4.5$, all of which are record values for spherical tokamaks.

The equilibria are well determined by the magnetic diagnostics, using a model which has been developed for the image currents in the thick START vacuum vessel. The equilibria are reconstructed using the EFIT equilibrium reconstruction code. All the equilibria for the record performance plasmas are vertically stable double null divertor discharges with elongation $\kappa\sim 2$.

The plasma termination is preceded by a $n=1$ magnetic precursor. Stability analysis of these discharges indicates stability to low-n ideal pressure driven kink modes. At the maximum β, the discharges are near marginal stability for the first ballooning stability boundary. Many of the discharges are also close to marginal stability to current driven ideal external kinks. Since the observed mode structure is observed to be low n, and the only low-n limit that is approached is the current driven kink limit, it is probable the disruptions are due to proximity to this low-q limit. Similar ohmic discharges with slightly higher values of q_{95} also disrupt, but at much lower plasma pressure with a strong relationship between q and l_i at the point of disruption.

There is reasonable agreement between the measured confinement of these plasmas and that predicted by the ITER97-Elmy scaling law. Measurements of the plasma density and temperature profiles for these high-β plasmas, along with calculations of the beam power deposition profiles, have been used to calculate the thermal diffusivities across the plasma profile. The results indicate that ion confinement is close to that predicted by neoclassical theory. The electron confinement is anomalous. These results should be compared to recent theoretical predictions of the confinement in spherical tokamaks, to begin to gain insight into the physics of confinement at low aspect ratio.

Certain of these plasmas exhibit features indicative of a change in transport regime. The global energy confinement is not strongly affected, but there are potential errors in the calculation of the energy confinement in such transient discharges. There is, however, clear evidence of broad profiles. There are also spikes in the $H\alpha$ emissions, similar to those observed coincident with ELMs in conventional divertor tokamaks in H-mode. Several other features are also observed, including: sharp edge electron density gradients, a reduction in the observed high-frequency magnetic fluctuations, and a drop in the overall level of $H\alpha$ emission. These changes in transport phenomenology are associated with improvements in vacuum conditioning techniques.

To be competitive, a spherical tokamak power plant will need to operate at higher β than a conventional tokamak, due to more stringent limitations on the maximum toroidal field on axis [taking this geometric consideration into account the $\beta_t=6.8\%$ achieved on Princeton Beta Experiment Modified (PBX-M)[15] at higher aspect ratio $A\sim 4$ is also an important high β result]. Therefore these results from START represent a significant achievement for spherical tokamak research. They indicate that the spherical tokamak concept is capable of supporting the normalized plasmas pressures in the range necessary for fusion applications. The stability of these record β discharges is most strongly correlated with the proximity to low safety factor boundaries. The energy confinement is on the order of that predicted by scaling laws

from conventional tokamak devices. Transport scaling has yet to be developed for spherical tokamaks, but these results are encouraging. Results from new larger scale experiments with longer pulse lengths that are currently under construction, such as the Mega-Amp Spherical Tokamak (MAST)[16] at Culham and the National Spherical Torus Experiment (NSTX)[17] at Princeton, should provide valuable information about the extent to which these results can be improved.

ACKNOWLEDGMENTS

This work was jointly funded by the UK Department of Trade and Industry and EURATOM. The EFIT code was provided by General Atomics, and the ERATO code by CRPP-Lausanne. The neutral beam injector is on loan from Oak Ridge National Laboratory/U.S. Department of Energy.

[1]Y.-K. M. Peng and D. J. Strickler, Nucl. Fusion **26**, 769 (1986).
[2]J. E. Menard, S. C. Jardin, S. M. Kaye, C. E. Kessel, and J. Manickam, Nucl. Fusion **37**, 595 (1997).
[3]A. Sykes, R. Akers, L. Appel, P. G. Carolan, N. J. Conway, M. Cox, A. R. Field, D. A. Gates, S. Gee, M. Gryaznevich, T. C. Hender, I. Jenkins, R. Martin, K. Morel, A. W. Morris, M. P. S. Nightingale, C. Ribiero, D. C. Robinson, M. Tournianski, M. Valovic, M. J. Walsh, and C. D. Warrick, in *Proceedings of the 24th European Conference on Controlled Fusion and Plasma Physics*, Berchtesgaden, 1997 (European Physical Society, Petit-Lancy, Switzerland, 1997), Vol. 1, p. 289.
[4]E. J. Strait, Phys. Plasmas **1**, 1415 (1994).
[5]M. J. Walsh, R. Akers, R. Buttery, D. Codling, N. Conway, M. Gryaznevich, T. Gunston, T. C. Hender, I. Jenkins, O. J. Kwon, R. Martin, M. Mironov, M. P. S. Nightingale, S. Petrov, C. Ribiero, D. C. Robinson, and R. T. C. Smith, in *Proceedings of the 23rd European Conference on Controlled Fusion and Plasma Physics*, Kiev, 1996 (European Physical Society, Petit-Lancy, Switzerland, 1996), Vol. 3, p. 1457.
[6]L. L. Lao, H. St. John, R. D. Stambaugh, A. G. Kellman, and W. Pfeiffer, Nucl. Fusion **25**, 1611 (1985).
[7]R. J. Buttery, M. K. Bevir, A. Caloutsis, D. Gates, C. G. Gimblett, M. Gryaznevich, T. C. Hender, I. Jenkins, R. Martin, C. Ribiero, D. C. Robinson, A. Sykes, M. Valovic, M. J. Walsh, and H. R. Wilson, in *Proceedings of the 23rd European Conference on Controlled Fusion and Plasma Physics*, Kiev, 1996 (European Physical Society, Petit-Lancy, Switzerland, 1996), Vol. 1, p. 416.
[8]J. A. Wesson, R. D. Gill, M. Hugon, F. C. Schuller, J. A. Snipes, D. J. Ward, D. V. Bartlett, D. J. Campbell, P. A. Duperrex, A. W. Edwards, R. S. Granetz, N. A. O. Gottardi, T. C. Hender, E. Lazarro, P. J. Lomas, N. Lopes Cardozo, K. F. Mast, M. F. F. Nave, N. A. Salmon, P. Smeulders, P. R. Thomas, B. J. D. Tubbing, M. F. Turners, and A. Weller, Nucl. Fusion **29**, 641 (1989).
[9]R. Gruber, F. Troyon, D. Berger, L. C. Bernard, S. Rousset, R. Schreiber, W. Kerner, W. Schneider, and K. V. Roberts, Comput. Phys. Commun. **21**, 323 (1981).
[10]ITER H-mode Database Working Group, Nucl. Fusion **34**, 131 (1994).
[11]P. G. Carolan, N. J. Conway, M. R. Tournianski, M. P. S. Nightingale, and M. J. Walsh, Plasma Phys. Rep. **24**, 206 (1998).
[12]G. V. Pereverzev, P. N. Yushmanov, A. Yu. Dnestrovskij, A. R. Polevoi, K. N. Tarajsan, and L. E. Zakharov, Kurchatov Institute of Atomic Energy Report, IAE-5358, 1992.
[13]C. M. Roach, Plasma Phys. Controlled Fusion **38**, 2187 (1996).
[14]K. Lackner and N. A. O. Gottardi, Nucl. Fusion **30**, 767 (1990).
[15]R. E. Bell, N. Askura, S. Bernmabei *et al.*, Phys. Fluids B **2**, 1271 (1990).
[16]A. C. Darke, in *Fusion Engineering*, Proceedings of the 16th Symposium Urbana-Champaign, 1995 (Institute of Electrical and Electronics Engineers, Piscataway, 1995), Vol. 2, p. 1456.
[17]J. Chrzanowski, H. Fan, P. Heitzenroeder, M. Ono, and J. Robinson, in Ref. 16, p. 1430.